

DYNAMIC STABILITY AND LINEAR VIBRATION ANALYSIS OF FUNCTIONALLY GRADED AXIALLY MOVING PIPES VIA THE FINITE ELEMENT APPROACH

¹Jiya M., ²Shaba A.I., ¹Yusuf A., ³Alhaji M.M. and ¹Bolarin G.

¹Department of Mathematics, Federal University of Technology, Minna, Nigeria
²Department of Applied Mathematics, Federal University of Technology, Babura, Nigeria
³Département de Civil Engineering, Federal University of Technology, Minna, Nigeria

*Corresponding Author Email Address: m.jiya@futminna.edu.ng

ABSTRACT:

This paper presents a finite element-based numerical investigation of the dynamic stability and linear vibration characteristics of an axially moving functionally graded pipe system. Functionally graded materials (FGMs) provide gradual variation in material properties, which can influence the structural response under axial motion. This study addresses the effects of axial speed and material gradation indices on natural frequencies and stability boundaries across five vibration modes. Numerical simulations show that increasing axial speed and gradation index leads to a reduction in natural frequencies with lower vibration modes being more sensitive due to combined geometric and material softening effects. A flutter instability is observed sharply beyond an axial speed of 40 m/s, indicating a dynamic instability threshold dependent on system parameters. Thermal stability analysis reveals that the system maintains robust resistance to temperature variations and changes in gradation indices. Harmonic response analysis identifies a dominant resonance peak near 5 Hz, characteristic of a lightly damped structure. These findings provide valuable guidance for the design and safe operation of advanced axially moving pipe systems in applications such as aerospace, mechanical conveyance and energy transport where stability and vibration control are critical.

Keywords: Functionally Graded Materials (FGM), Dynamic Stability, Finite Element Method (FEM), Linear Vibration Analysis, axially moving Pipe.

Nomenclature

| | |
|------------|-------------------------------------|
| $w(x, t)$ | Displacement |
| L | Length of the pipe |
| $\rho(x)$ | Density distribution along the pipe |
| v | Axial velocity |
| e_{31} | piezoelectric coupling Coefficient |
| T_0 | Initial axial tension |
| α | Thermal expansion coefficient |
| ΔT | Temperature difference |
| K_f | Foundation stiffness |
| A | Sectional Area |

| | |
|--------|--------------------------------|
| $I(x)$ | Moment of inertia distribution |
| $E(x)$ | Young's modulus distribution |

INTRODUCTION

Axially moving pipes are integral to engineering applications across aerospace, marine and manufacturing industries where they are used for conveying materials such as paper webs, cables and fuel lines. These structures often experience complex dynamics due to the coupling between axial motion and transverse vibration making their stability and vibratory behaviour critical for ensuring operational safety and performance.

Early studies laid the foundation for understanding the dynamics of axially moving structures. Paidoussis and Issid (1974) and Wickert and Mote (1978) pioneered theoretical analyses of the dynamics and stability characteristics of such systems. However, advances in material design have reshaped this field. Functionally graded materials (FGMs) with spatially tailored mechanical and thermal properties (Miyamoto *et al.*, 1999) have demonstrated significant benefits for engineering structures subject to thermal and mechanical loading. Despite their promise, the application of FGMs to axially moving pipes has remained largely underexplored.

More recent studies have addressed dynamics in the context of FGM beams and pipes. Cui and Zhang (2024) analysed buckling behaviour of axially loaded FGM beams highlighting the role of the gradient index and boundary conditions in determining critical loads. Mao *et al.* (2023) examined the nonlinear dynamics of FGM pipes conveying fluid finding that material gradation significantly influences natural frequencies and equilibrium configurations. Jing *et al.* (2024) extended this approach to parametric resonance in FGM pipes with pulsating flow identifying critical instability regions associated with the gradient index and flow velocity. Fu *et al.* (2024) further incorporated gas-liquid two-phase flow effects, revealing complex frequency characteristics and critical flow velocities shaped by FGM gradation and constraints.

Additional studies have contributed valuable insights into related areas of dynamics. For instance, Shaba *et al.* (2021) examined vibration behaviour of single-walled carbon nanotubes resting on Winkler foundations with magnetic effects, providing a foundation for understanding the interaction of external fields and nanobeam dynamics. Jiya and Shaba (2018) analysed the dynamics of Bernoulli-Euler beams resting on Winkler foundations and subjected to moving loads, while Jiya *et al.* (2018) performed a dynamic response analysis of fluid-conveying pipes resting on Pasternak foundations. These studies deepen the understanding

of complex fluid–structure interactions and external constraints but largely focus on fluid–structure coupling and nonlinear effects, rather than the behaviour of purely axially moving FGM pipes.

Although prior studies have advanced the understanding of FGM beams and fluid–structure dynamics, none have explicitly addressed the dynamics of purely axially moving FGM pipes. The unique contribution of this work lies in its comprehensive modelling of an axially moving pipe composed of FGM material. Unlike prior analyses (Paidoussis & Issid, 1974) that considered axial motion but ignored material gradation, or FGM studies that incorporated fluid–structure interaction (Mao *et al.*, 2023; Jing *et al.*, 2024; Fu *et al.*, 2024), this paper develops a robust Finite Element Model (FEM) that captures the coupled axial–transverse dynamics of FGM pipes. The approach includes centrifugal and Coriolis effects induced by axial motion utilizing a six-degree-of-freedom beam element that captures axial displacement, transverse deflection and rotational inertia.

The primary objective of this study is to investigate how a power-law FGM gradation influences the natural frequencies, mode shapes and stability thresholds of axially moving pipes. By addressing this gap, the research provides valuable insights for designing next-generation axially moving structures (e.g., cables, pipelines or aerospace fuel lines) with enhanced stability and performance. In doing so, it aims to advance the state of knowledge and engineering practice for this critical area of study.

PROBLEM FORMULATION

The problem under consideration a functionally graded pipe moving axially on elastic medium as shown in Figure 1. In formulation of the model, the following assumption were made:

1. The pipe moves axially on a continuous elastic foundation
2. Transverse displacement is assumed to be small so that Euler – Bernoulli Beam Theory (EBBT) is applied
3. Smart Material Effect (Piezoelectric Coupling).
4. Thermal load is applied
5. Thin – walled assumption so that shear deformation is neglected.
6. Pipe Gyroscopic (Coriolis) effect considered
7. Initial axial Tension
8. No internal fluid flow (pure axial translation)
9. Simply supported boundary condition

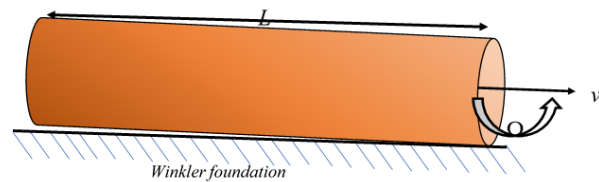


Figure 1: Schematic diagram of Functionally Graded Pipe (FGP) moving axially

The Kinetic energy of the pipe includes contributions from transverse and axial motion given as:

$$T = \frac{1}{2} \int_0^L \rho(x) A \left(\frac{\partial w}{\partial t} + v \frac{\partial w}{\partial x} \right)^2 dx \quad (1)$$

And Potential Energy of the pipe include Bending strains energy, axial tension, foundation stiffness, thermal energy and smart material energy given below

Bending strains energy

$$V_b = \frac{1}{2} \int_0^L E(x) I(x) \left(\frac{\partial^2 w}{\partial x^2} \right)^2 dx \quad (2)$$

Axial tension

$$V_T = \frac{1}{2} \int_0^L T_0 \left(\frac{\partial w}{\partial x} \right)^2 dx \quad (3)$$

Foundation stiffness

$$V_F = \frac{1}{2} \int_0^L k_f w^2 dx \quad (4)$$

Thermal Energy

$$V_\theta = \frac{1}{2} \int_0^L E(x) \alpha A \Delta T \left(\frac{\partial w}{\partial x} \right)^2 dx \quad (5)$$

Smart material energy

$$V_S = \frac{1}{2} \int_0^L e_{31} \left(\frac{\partial w}{\partial x} \right)^2 dx \quad (6)$$

Total Potential Energy is

$$V = V_b + V_T + V_F + V_\theta + V_S \quad (7)$$

$$V = \frac{1}{2} \int_0^L \left[E(x) I(x) \left(\frac{\partial^2 w}{\partial x^2} \right)^2 + T_0 \left(\frac{\partial w}{\partial x} \right)^2 + k_f w^2 + E(x) \alpha A \Delta T \left(\frac{\partial w}{\partial x} \right)^2 + e_{31} \left(\frac{\partial w}{\partial x} \right)^2 \right] dx \quad (8)$$

By Hamilton's Principle

$$\delta \int_{t_1}^{t_2} (T - V) dx = 0 \quad (9)$$

Integrating by parts and applying boundary condition, the Euler – Lagrange equation yield as below

$$\left. \frac{\partial^2}{\partial x^2} \left(E(x) I(x) \frac{\partial^2 w}{\partial x^2} \right) + \rho(x) A \frac{\partial^3 w}{\partial t^2} + 2\rho(x) A v \frac{\partial^2 w}{\partial x \partial t} + (T_0 - \rho(x) A v^2 - E(x) \alpha A \Delta T - e_{31}) \frac{\partial^2 w}{\partial x^2} \right\} + K_f w = 0 \quad (10)$$

Where

$$E(x) = (E_m + (E_c - E_m)) \left(\frac{x}{L} \right)^n \quad (11)$$

$$\rho(x) = (\rho_m + (\rho_c - \rho_m)) \left(\frac{x}{L} \right)^n \quad (12)$$

$$I(x) = (I_m + (I_c - I_m)) \left(\frac{x}{L}\right)^n \quad (13)$$

Initial condition

$$w(x, 0) = w'(x, 0) = 0 \quad (14)$$

Boundary condition (Simply – Supported)

$$w(0, t) = w(L, t) = 0 \quad (15)$$

$$\left. \frac{\partial^2 w}{\partial x^2} \right|_{x=0} = 0, \quad \left. \frac{\partial^2 w}{\partial x^2} \right|_{x=L} = 0 \quad (16)$$

FINITE ELEMENT FORMULATION

The Entire pipe is discretized into 2D beam element (Frame). Each element is a two – node clamped – clamped (C – C) beam element with each having three (3) degree of freedom (DOF). Two are longitudinal (axial) displacement, u_1 & u_4 ; two are transverse (lateral) displacement, u_3 & u_6 and the remaining two are rotational (angular) displacement, u_2 & u_5 as shown in Figure 2 below

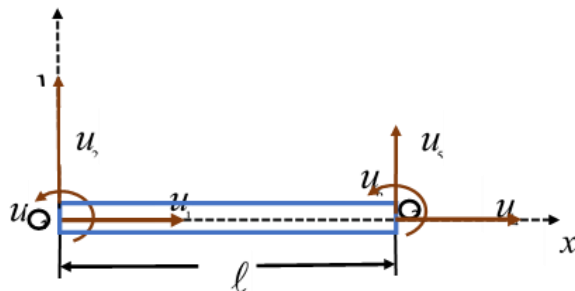


Figure 2: A Two – node Beam Element.

The axial displacement uses linear interpolation (Lagrange 2 – node) as

$$\left. \begin{aligned} N_1 &= \left(1 - \frac{x}{l}\right) \\ N_4 &= \frac{x}{l} \end{aligned} \right\} \quad (17)$$

While transverse and rotational displacement use Hermite cubic beam interpolation as

$$\left. \begin{aligned} N_2 &= 1 - \frac{3x^2}{l^2} + \frac{2x^3}{l^3} \\ N_3 &= x - \frac{2x^2}{l} + \frac{x^3}{l^2} \\ N_5 &= \frac{3x^2}{l^2} - \frac{2x^3}{l^3} \\ N_6 &= \frac{x^3}{l^2} - \frac{x^2}{l} \end{aligned} \right\} \quad (18)$$

SOLUTION OF THE MODEL

Assume solution of the form

$$w(x, t) = \begin{bmatrix} w_1(x, t) \\ w_2(x, t) \end{bmatrix} = \sum_{i=1}^6 N_i(x) U_i(t) \quad (19)$$

$$\text{Where } N_i(x) = \begin{bmatrix} N_1 & 0 & 0 & N_4 & 0 & 0 \\ 0 & N_2 & N_3 & 0 & N_5 & N_6 \end{bmatrix} \quad (20)$$

$$U_i(t) = \begin{bmatrix} u_1 \\ u_2 \\ u_3 \\ u_4 \\ u_5 \\ u_6 \end{bmatrix} \quad (21)$$

Applying Galerkin weak formulation to equation (10) by multiply shape function $N_i^T(x)$ and integrate over the domain $(0, l)$

$$\int_0^l \left[\begin{aligned} & \frac{\partial^2}{\partial x^2} \left(\left((E_m + (E_c - E_m)) \left(\frac{x}{L} \right)^n \right) I \frac{\partial^2 w}{\partial x^2} \right) + \left((\rho_m + (\rho_c - \rho_m)) \left(\frac{x}{L} \right)^n \right) A \frac{\partial^2 w}{\partial t^2} + \\ & 2 \left((\rho_m + (\rho_c - \rho_m)) \left(\frac{x}{L} \right)^n \right) A v \frac{\partial^2 w}{\partial x \partial t} + \\ & \left(T_0 - \left((\rho_m + (\rho_c - \rho_m)) \left(\frac{x}{L} \right)^n \right) A v^2 \right) \frac{\partial^2 w}{\partial x^2} + K_f w \\ & - \left((E_m + (E_c - E_m)) \left(\frac{x}{L} \right)^n \right) \alpha A \Delta T - e_{31} \end{aligned} \right] dx = 0 \quad (22)$$

After applying integration by part and boundary condition, we have

$$[M] \ddot{U}(t) + [G] \dot{U}(t) + [K] U(t) = 0 \quad (23)$$

Where

$$[M] = A \int_0^L \left((\rho_m + (\rho_c - \rho_m)) \left(\frac{x}{L} \right)^n \right) N^T(x) N(x) dx \quad (24)$$

$$[G] = (2vA) \int_0^L \left((\rho_m + (\rho_c - \rho_m)) \left(\frac{x}{L} \right)^n \right) N^T(x) \frac{dN(x)}{dx} dx \quad (25)$$

$$[K] = \left\{ \begin{aligned} & \int_0^L \left((E_m + (E_c - E_m)) \left(\frac{x}{L} \right)^n \right) I N''(x) N(x) dx + \\ & \left(T_0 - \left((\rho_m + (\rho_c - \rho_m)) \left(\frac{x}{L} \right)^n \right) A v^2 - \right. \\ & \left. \int_0^L \left((E_m + (E_c - E_m)) \left(\frac{x}{L} \right)^n \right) \alpha A \Delta T - e_{31} \right) N^T(x) N''(x) dx + K_f \int_0^L N^T(x) N(x) dx \end{aligned} \right\} \quad (26)$$

Because the material properties vary with x analytical integration is complicated, so numerical integration is applied using two – point Gauss quadrature. MATLAB software is used to assemble all element matrices into global matrices and eigenvalue problem for free vibration is solved as in this equation:

$$([K] - \omega^2 [M] + j\omega [G]) \phi = 0 \quad (27)$$

RESULTS AND DISCUSSIONS

The eigenvalue problem with free vibration is solved with MATLAB software. To simulate the model the following assumed data were used from literature. $L = 20m$, $I = 8.33 \times 10^{-10}$, $E_m = 2 \times 10^{11}$, $E_c = 5 \times 10^{11}$, $\rho_m = 7800$, $\rho_c = 3200$, $\Delta T = 50$, $\alpha = 1 \times 10^{-5}$, $T_0 = 1 \times 10^4$, $K_f = 1000$, $e_{31} = 1$

The natural frequencies of the axially moving functionally graded

pipe system were evaluated for multiple gradation indices and five vibration modes under varying material gradation. With 10 elements. The obtained results for each gradation index are presented in Tables 1 to 4

Table 1: Natural frequencies for gradation $n = 0$

| Mode 1 | Mode 2 | Mode 3 | Mode 4 | Mode 5 |
|--------|--------|--------|--------|--------|
| 6.0771 | 7.5294 | 7.8957 | 8.0304 | 8.0925 |
| 6.0575 | 7.5145 | 7.8827 | 8.0183 | 8.081 |
| 5.9991 | 7.4701 | 7.8436 | 7.982 | 8.0466 |
| 5.9038 | 7.3969 | 7.7789 | 7.9212 | 7.9883 |
| 5.7737 | 7.2958 | 7.6886 | 7.8356 | 7.9053 |

Table 1 shows that the natural frequencies of all modes decrease slightly. For Mode 1, frequency reduces from 6.0771 Hz to 5.7737 Hz. A similar pattern is observed across all five modes. Increasing axial speed leads to a gradual decrease in vibrational frequencies. The reduction is more significant in lower modes (Mode 1 and Mode 2), while higher modes remain relatively stable.

Table 2: Natural frequencies for gradation $n = 1$

| Mode 1 | Mode 2 | Mode 3 | Mode 4 | Mode 5 |
|--------|--------|--------|--------|--------|
| 3.469 | 3.849 | 4.2253 | 4.2957 | 4.6462 |
| 3.4401 | 3.8224 | 4.211 | 4.2411 | 4.6251 |
| 3.3555 | 3.7408 | 4.1017 | 4.1402 | 4.5602 |
| 3.2211 | 3.5981 | 3.8611 | 4.0161 | 4.4481 |
| 3.0458 | 3.3806 | 3.4987 | 3.8326 | 4.2836 |

Compared to Table 1, Table 2 represents a system with a different (higher) gradation index. The absolute values of natural frequencies are noticeably lower across all modes. For instance, Mode 1 reduces from 3.469 Hz to 3.0458 Hz as axial speed increases. The consistent reduction across modes reflects the joint influence of axial movement and gradation. The lower absolute frequencies confirm that increasing gradation index introduces more compliant (less stiff) material into the structure, reducing its dynamic stiffness.

Table 3: Natural frequencies for gradation $n = 2$

| Mode 1 | Mode 2 | Mode 3 | Mode 4 | Mode 5 |
|--------|--------|--------|--------|--------|
| 3.0658 | 3.3621 | 3.5319 | 3.7913 | 3.9444 |
| 3.0279 | 3.3339 | 3.5048 | 3.7658 | 3.899 |
| 2.9189 | 3.2468 | 3.4206 | 3.6869 | 3.7601 |
| 2.7482 | 3.0941 | 3.2708 | 3.5182 | 3.5478 |
| 2.5227 | 2.8602 | 3.0434 | 3.1523 | 3.3388 |

In Table 3, a further increase in gradation index results in a more compliant structure. The first mode frequency ranges from 3.0658 Hz to 2.5227 Hz. As before, all higher modes follow the same decreasing trend. The relatively larger drop in Mode 1 suggests that fundamental modes are most sensitive to both axial motion and gradation variations. This behaviour aligns with the theoretical understanding of functionally graded structures where material softening affects the first few modes more prominently.

Table 4: Natural frequencies for gradation $n = 3$

| Mode 1 | Mode 2 | Mode 3 | Mode 4 | Mode 5 |
|--------|--------|--------|--------|--------|
| 2.8868 | 3.2759 | 3.3395 | 3.4679 | 3.7036 |
| 2.8448 | 3.246 | 3.3119 | 3.4406 | 3.6777 |
| 2.7249 | 3.1558 | 3.2245 | 3.3552 | 3.5971 |
| 2.5386 | 3.0033 | 3.0649 | 3.202 | 3.4542 |
| 2.294 | 2.7831 | 2.8103 | 2.9675 | 3.108 |

Table 4 presents the most compliant case (highest gradation index among these cases). The Mode 1 frequency ranges from 2.8868 Hz to 2.2940 Hz, while Mode 5 reduces from 3.7036 Hz to 3.1080 Hz. The significant reduction in frequencies across all modes demonstrates that as the softer constituent dominates the material composition, the structural stiffness reduces, leading to significant frequency drops even at relatively low system parameters.

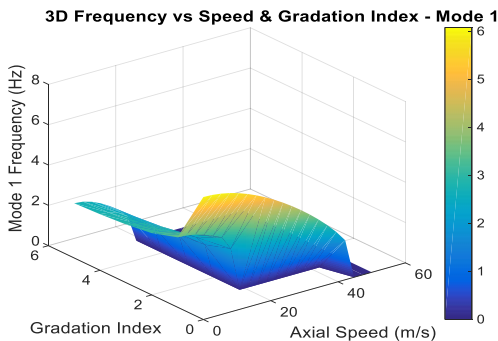


Figure 3: Graph of frequency against speed and gradation index mode 1

Figure 3 illustrates the combined effect of axial speed and gradation index on the Mode 1 natural frequency. Both increasing axial speed and gradation index lead to a significant reduction in natural frequencies primarily due to the combined influence of centrifugal softening and reduced material stiffness. The nonlinearity in the surface curvature reflects strong coupling between the two parameters revealing a progressive approach towards instability at high axial speeds and high gradation levels.

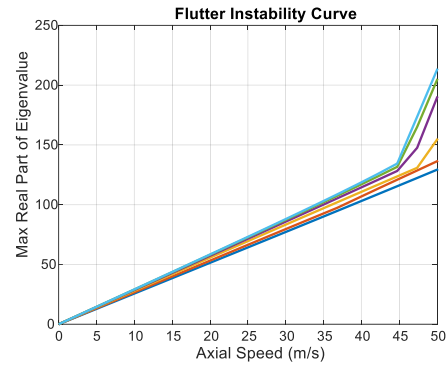


Figure 4: Flutter instability curve

Figure 4 presents the flutter instability curve based on the real part of the eigenvalues. Stability is maintained up to approximately 40 m/s, beyond which a rapid increase in the real part signals the onset of instability. The system exhibits different instability thresholds depending on the gradation index, confirming that material softening accelerates instability under higher speed.

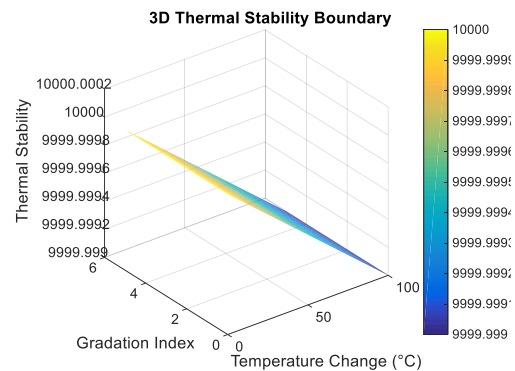


Figure 5: thermal stability boundary curve

Figure 5 shows that thermal stability remains nearly constant around 9999.999 across the tested gradation index (0–6) and temperature change (0–100°C). This indicates excellent thermal robustness, as the effect of temperature-induced softening is negligible within the studied range. Thus, thermal loading does not significantly compromise dynamic stability for the FG pipe system in this context.

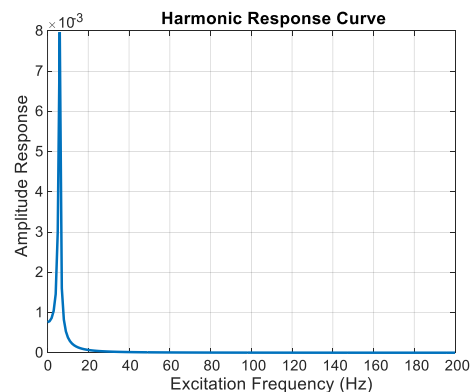


Figure 6: Harmonic response curve

Figure 6 displays the harmonic response, revealing a dominant resonance peak around 5 Hz. The sharpness of the peak suggests a lightly damped system, which may experience significant vibrational amplitudes under resonant excitation. Such behavior underscores the need to consider damping mechanisms in practical designs, particularly for operational conditions near the natural frequency

Conclusion

This study presents a comprehensive numerical investigation of the dynamics of an axially moving functionally graded (FG) pipe yielding critical insights into its vibratory behaviour. The results clearly demonstrate that increasing axial speed causes a significant and consistent reduction in natural frequencies across all vibration modes, with the lower modes being especially sensitive. Moreover, higher material gradation indices indicative of softer material compositions further depresses the absolute values of the natural frequencies especially in the fundamental modes. The combined effects of higher gradation and increased axial velocity precipitate a sharp decline in natural frequencies and a trend towards dynamic instability as evidenced by the rising real part of the eigenvalues beyond approximately 40 m/s.

Interestingly, thermal effects within the examined range have only a negligible influence on the dynamics, suggesting robust thermal stability across the considered temperatures. The pipe also exhibits characteristics akin to a lightly damped structure, as evidenced by its distinct resonance peaks at low excitation frequencies.

While these findings illuminate the interplay between material gradation, axial motion, and vibratory behaviour, this study is not without its limitations. The analysis is restricted to linear vibration theory and excludes nonlinear dynamics and fluid–structure interaction effects that arise in many engineering applications. Additionally, the thermal investigation was confined to a limited range of temperatures and material profiles, leaving scope for further exploration of thermal–structural coupling and complex FGM compositions. Nonetheless, the results underscore the importance of informed design and parameter optimization for ensuring the long-term stability and reliability of axially moving FG structures.

Recommendations

1. Careful consideration should be given to selecting the FGM gradation index as higher indices reduce natural frequencies and may compromise dynamic stability especially under higher axial speeds.
2. Identify and implement critical axial velocity limits for different material gradation indices to mitigate the risk of dynamic instability and catastrophic failures.
3. As the system behaves like a lightly damped structure employ damping treatments or design interventions to shift natural frequencies away from common excitation ranges and reduce resonance risk.
4. Perform in-depth analyses of nonlinear surface curvature, complex material compositions and high gradation profiles to more accurately define the stability boundaries and dynamic behaviour of FGM pipes at critical speeds.
5. Broaden thermal investigations to encompass higher temperatures and varied FGM compositions providing a more comprehensive understanding of thermal–

structural coupling and its role in long-term performance and reliability.

Acknowledgement

The authors want to acknowledge the financial support provided by the Tertiary Education Trust Fund (TETFund) through the Institutional Based Research Grant (TETFUND/FUTMINNA/2024/018) which made this research work possible

REFERENCE

- Cui, S., & Zhang, Y. (2024). *Stability analysis of axially functionally graded beams using the differential quadrature method*. *Advances in Applied Mathematics and Mechanics*, 16(5), 1039–1055. <https://doi.org/10.4208/aamm.OA-2023-0087>
- Fu, G., Wang, X., Wang, B., Su, J., Wang, K., & Sun, B. (2024). *Dynamic behavior of axially functionally graded pipe conveying gas–liquid two-phase flow*. *Applied Ocean Research*, 142, Article 103827. <https://doi.org/10.1016/j.apor.2023.103827>
- Jing, J., Mao, X., Ding, H., & Chen, L. (2024). *Parametric resonance of axially functionally graded pipes conveying pulsating fluid*. *Applied Mathematics and Mechanics–English Edition*, 45, 239–260. <https://doi.org/10.1007/s10483-024-3083-6>
- Jiya, M. & Shaba, A. I. (2018). *Analysis of a Uniform Bernoulli – Euler Beam on a Winkler foundation subjected to harmonic moving load*. *Journal of Applied Science and Environmental Management*, 22(3), 368 – 372.
- Jiya, M., Inuwa, Y. I. & Shaba, A. I. (2018). *Dynamic response analysis of a Uniform Conveying fluid pipe on two – parameter elastic foundation*. *Science World Journal*, 13(2), 1 – 5.
- Mao, X.-Y., Jing, J., Ding, H., & Chen, L.-Q. (2023). *Dynamics of axially functionally graded pipes conveying fluid*. *Nonlinear Dynamics*, 111, 11023–11044. <https://doi.org/10.1007/s11071-023-08470-2>
- Miyamoto, Y., Kaysser, W. A., Rabin, B. H., Kawasaki, A., & Ford, R. G. (1999). *Functionally graded materials: Design, processing and applications*. Springer.
- Paidoussis, M. P., & Issid, N. T. (1974). *Dynamic stability of pipes conveying fluid*. *Journal of Sound and Vibration*, 33(3), 267–294.
- Shaba, A. I., Jiya, M., Aiyesimi, Y. M., & Mohammed, A. A. (2021). *Vibration of Single – walled carbon nanotube (SWCNT) on a Winkler foundation with magnetic effect*. *Science World Journal*, 16(4), 402 – 406.
- Wickert, J., & Mote, C. D. (1978). *Stability and vibration of translating beams*. *Journal of Sound and Vibration*, 58(3), 467–482.